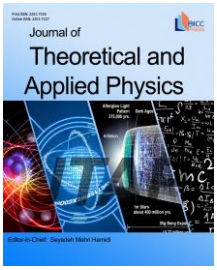

J. Theor. Appl. Phys., 2026; 20(2): 152-166

Journal of Theoretical and Applied Physics (JTAP)

https://doi.org/10.57647/jtap.2026.2002.15

Research Article

Disentangling Thermal and Degeneracy Pressure in Quantum-Confined Fermi Gases

Coskun Firat*

Istanbul Technical University, Energy Institute, Istanbul, Turkey

***Corresponding author:** coskun.firat@itu.edu.tr

Article History:

Received:
14 October 2025

Revised:
15 November 2025

Accepted:
17 December 2025

Published Online:
05 February 2026

Published in Issue:
30 April 2026

Abstract

A theoretical framework is developed to decompose the total pressure of a quantum-confined Fermi gas into degeneracy pressure, arising from Fermi–Dirac statistics, and thermal pressure, associated with finite-temperature excitations. Using Weyl's conjecture for the confined density of states, geometric confinement effects are incorporated through surface- and edge-to-volume parameters (α and β). Exact analytical expressions for both components are derived using polylogarithmic functions, and asymptotic forms are obtained for the strongly degenerate ($T \ll T_F$) and weakly degenerate ($T \gg T_F$) regimes. The analysis shows that quantum confinement enhances degeneracy pressure by a factor of $(1 + 5\alpha^F/16)$, while suppressing thermal pressure, with the contrast most significant under strong degeneracy. The maximum relative error in the total pressure, occurring at the crossover temperature $\tilde{T}^* \sim 0.604282$, is about 22%, while that for thermal pressure reaches 52%. The asymptotic expressions remain valid across $\alpha^F \in [0.1, 0.5]$ and $\beta^F \in [0.01, 0.2]$. Separating thermal and degeneracy contributions enables improved interpretation of thermodynamic measurements in confined quantum systems where only total pressure is accessible. The framework is relevant for nanoelectronic devices, ultracold atomic gases, and quantum dots, offering insight into how spatial confinement differentially shapes thermal and quantum contributions to observable thermodynamic behavior.

Keywords: Fermions, Thermal pressure, Degeneracy pressure, Quantum size effects, Confined quantum systems, Equation of state

Cite this article: Firat, C., (2026). Disentangling Thermal and Degeneracy Pressure in Quantum-Confined Fermi Gases. *J. Theor. Appl. Phys.,* 20(2), 152-166. https://doi.org/10.57647/jtap.2026.2002.15

1. Introduction

Pressure, defined as force per unit area, is fundamentally determined by two distinct mechanisms: thermal pressure and degeneracy pressure.

While thermal pressure dominates ordinary gases via the kinetic energy of particles at non-zero temperatures, degeneracy pressure arises from quantum mechanical effects, primarily the Pauli exclusion principle, becoming crucial in high-density or low-temperature fermionic systems.

Distinguishing between these two forms of pressure is essential for understanding their individual and combined influences on matter.

Thermal pressure stems from particle kinetic energy due to thermal activity, leading to the classical ideal gas law:

$$PV = Nk_bT \quad (1)$$

where pressure (P) scales linearly with temperature (T) and particle density. Kinetic energy not originating from thermal sources, such as zero-point energy, does not contribute to thermal pressure. In contrast, degeneracy pressure acts as an anti-compression force in fermionic systems by forcing particles into higher energy levels due to quantum mechanics and the Pauli exclusion principle. This pressure is crucial for how fermionic systems act in extreme settings. Unlike thermal pressure, it is not significantly affected by low temperatures and remains important even at absolute zero. In quantum gases, thermal pressure contributes to the formation and stability of Bose–Einstein condensates, although it becomes negligible within the condensed phase itself. At sufficiently low temperatures, degeneracy pressure emerges as a key factor, but its behavior differs markedly between Fermi and Bose systems. In Fermi gases, the Pauli exclusion principle causes degeneracy pressure to dominate, thereby increasing the total pressure. In contrast, for Bose gases, degeneracy leads to a reduction in pressure as particles increasingly occupy the ground state, and the total pressure can even fall below that of a classical gas as the temperature decreases. This distinction underscores the fundamentally different roles played by degeneracy pressure in Fermi and Bose gases, with the bosonic character giving rise to a unique form of degeneracy pressure that governs the behavior of Bose–Einstein condensates [1–7]. In confined nanoscale systems, the interaction between pressure and boundaries is governed by quantum size effects (QSE), which become significant when the thermal wavelength is comparable to the system dimensions [8-23]. QSE alters the density of states (DOS), causing the thermodynamic behavior to deviate from the classical bulk limit, where the system is unbounded and the Maxwell-Boltzmann distribution applies [24]. By classical, we refer to the ideal gas behavior in the unbounded state. The analysis of QSE in confined Fermi gases is driven by incorporating geometric corrections, such as surface-to-volume (α) and edge-to-volume (β) confinement parameters, into thermodynamic properties [8–14, 21, 24]. The theoretical foundation is rooted in the spectral theory of the Laplacian operator, which is complemented by related work on inverse spectral problems [10, 27-30]. In 1911, Weyl provided the initial mathematical framework, demonstrating that the asymptotic distribution of single-particle energy eigenvalues depends not only on the domain's volume but also on geometric properties, specifically surface area [25]. This approach, known as Weyl's conjecture, was mathematically established in [26] and is rigorously validated for domains with smooth boundaries [31-37].

This study advances current understanding by explicitly decomposing the total pressure in confined nanoscale systems into its thermal and degeneracy contributions. In contrast with earlier approaches that focus solely on the total pressure, the present work isolates the thermal component by subtracting the zero-temperature (degeneracy) limit from polylogarithmic expressions. The analysis reveals that quantum confinement affects these two contributions differently: it enhances the degeneracy pressure while suppressing the thermal pressure, with the contrast becoming especially pronounced under strong degeneracy conditions. New asymptotic formulations are developed for both the high- and low-degeneracy regimes. By distinguishing the individual pressure components, the framework provides deeper insight into systems where only the total pressure is experimentally accessible, allowing for a clearer understanding of how geometric confinement influences each contribution. This separation is particularly relevant for applications in nanoelectronic devices and ultracold atomic traps, where precise thermodynamic control is essential.

2. Fermi gas confined in a nano scale domain

Spatial restrictions in nanoscale systems quantize energy levels by limiting particle motion. This quantization changes the density of states, affecting thermal and quantum pressure. Fermi-Dirac statistics apply to Fermi gases, but confinement alters particle energy state occupancy.

Quantum influences are major at low temperatures or high densities, with thermal excitation rising at high temperatures or low densities. In statistical mechanics, approximating infinite system volume to sum over all states loses geometric details. The state count becomes volume-proportional, ignoring boundary shape. This simplification may neglect boundary effects on particle behavior, especially in confined systems [35]. System properties rely heavily on geometry and topology, particularly at the nanoscale where confinement causes unique phenomena.

Geometry's influence on physical behavior helps us understand how systems work at this scale. This understanding can guide the creation of new tech with specific geometric designs [36-40]. When the de Broglie wavelengths of particles are not negligible compared to the dimensions of the confinement domain, then the density of states needs to be determined much more precisely. It is first conjectured by Weyl that, the number of eigenvalues of the Helmholtz equation given by Eq. (2), smaller than a given asymptotic eigenvalue k, is represented by the Eq. (3) as the counting function (Weyl's conjecture) [9, 18, 21, 41-44];

$$\nabla^2\psi(\mathbf{x}) + k^2\psi(\mathbf{x}) = 0 \tag{2}$$

$$\Omega_{D\leq 3}(k) = \frac{Vk^3}{6\pi^2}\Theta(D-3) + \frac{(-1)^D Ak^2}{4^{D-2}4\pi}\Theta(D-2) + \frac{(-1)^{D-1}Ck}{4^{D-1}\pi}\Theta(D-1) + \frac{(-1)^{D-2}N_V}{4^D}\Theta(k) \tag{3}$$

Here, V is the volume, A is the surface area, C is the perimeter and N_v is the corners and the holes of the box, $\hbar$ is the reduced Planck's constant and $\Theta(x)$ is Heaviside step function which is equal to 1 for $x \geq 0$ and 0 otherwise, and D represents the dimension of the domain. The dispersion relationship between wavenumbers and energy eigenvalues as, $k = \sqrt{2m\varepsilon}/\hbar$, m is the mass of the particles. Eq. (3) includes not only the volume, V, that dominates, but also surface area, A, edge, C, and corners and holes, N_V, corrections, reflecting the finite size effects and the boundary conditions. By considering the dispersion relationship, the Eq. (3) takes the following form for D = 3:

$$\Omega_{D=3}(\varepsilon) = \frac{V(2m\varepsilon)^{3/2}}{6\pi^2\hbar^3} - \frac{A(2m\varepsilon)}{16\pi\hbar^2} + \frac{C\sqrt{2m\varepsilon}}{16\pi\hbar} - \frac{N_V}{64}\Theta(\varepsilon) \tag{4}$$

Using the Weyl's conjecture, the density of states $g(\varepsilon)$ is obtained as the derivative of the counting function $\Omega_{D=3}(\varepsilon)$ with respect to the energy ε. For D=3, the density of states function is obtained as the below:

$$g(\varepsilon) = \frac{d\Omega_3(\varepsilon)}{d\varepsilon} = \frac{V}{\sqrt{2}\pi^2}\frac{m^{3/2}}{\hbar^3}\sqrt{\varepsilon} - \frac{A}{8\pi}\frac{m}{\hbar^2} + \frac{C}{16\sqrt{2}\pi}\frac{\sqrt{m}}{\hbar}\frac{1}{\sqrt{\varepsilon}} - \frac{N_V}{128}\frac{\sqrt{m}}{\hbar}\frac{1}{\sqrt{\varepsilon}}.\delta\left(\sqrt{m\varepsilon}/\hbar\right) \tag{5}$$

where, $\delta\left(\sqrt{m\varepsilon}/\hbar\right)$ is Dirac Delta function. Eq. (5) represents the number of states per unit energy interval.

For macroscopic or mesoscopic systems where $N_V \ll N$ (number of particles), this contribution is negligible compared to volume, surface, and edge terms. In typical 3D nanostructures, $N_V \approx 8$ (e.g., corners of a rectangular box), while $N \approx 10^3 - 10^6$, so the relative contribution is $< 10^{-3}$. Thus, we omit this term in subsequent thermodynamic integrations (Eqs. 6-13) without loss of accuracy for the parameter regimes considered. In Eq. (5), it is assumed that the density of states is continuous. Hence, in a system in thermodynamic equilibrium, the number of particles expression obeying the Fermi-Dirac (FD) statistics given in Eq. (6), is obtained by an integral expression as:

$$N = \sum_r \frac{1}{\exp[(\varepsilon_r - \mu)/k_bT] + 1} \approx \int_0^\infty \frac{g(\varepsilon)d\varepsilon}{\exp\left[\frac{\varepsilon}{k_bT} - \Lambda\right] + 1} \tag{6}$$

Here the index r is the generalized quantum state index and $\Lambda = \mu/k_bT$. Notably, all quantities has been divided by spin degree of freedom ($g_s = 2$ for electrons). To calculate the summation in Eq. (6) over all quantum states needs to know energy eigenvalues ε_r. When ε_r known then the summation in Eq. (6) could be performed exactly by use of the Euler-MacLaurin formula [45]:

$$\sum_{n=0}^{\infty} F(n) = \int_0^\infty F(n)dn + \frac{1}{2}F(0) - \frac{1}{2!}B_2F'(0) - \frac{1}{4!}B_4F'''(0) + \cdots \tag{7}$$

Since it is not possible to determine the energy eigenvalues analytically for an arbitrarily shaped domain to handle the summation in Eq. (6), then Eq. (5), derived from Weyl's conjecture, provides a reliable approximation to the asymptotics of eigenvalues.

This allows us to replace the infinite summation with an integral in Eq. (6). This approach effectively addresses the challenges posed by complex geometries, allowing for meaningful insights into the system's thermodynamic properties. When integral in the Eq. (6) is taken using Eq. (5), the number of particles for a Fermi gas confined in a 3D, arbitrary shaped domain is obtained as follows which is also consistent with the literature [21, 24]:

$$N = -\frac{\pi^{3/2}V}{8L_c^3}Li_{3/2}(-e^{\Lambda}) + \frac{\pi}{2}\frac{A}{8L_c^2}Li_1(-e^{\Lambda}) - \frac{\sqrt{\pi}}{2}\frac{C}{16L_c}Li_{1/2}(-e^{\Lambda}) \tag{8}$$

In this expression, $Li_m[.]$ are poly-logarithmic functions [46], $L_c = h/2\sqrt{2mk_bT} = \sqrt{\pi}\lambda_{th}/2$ is the half of the most probable de Broglie wavelength of the particles and $\lambda_{th} = h/\sqrt{2\pi mk_bT}$ is the thermal de Broglie wavelength of the particles.The grand canonical potential, ϕ, sometimes called the Landau free energy, provides a linkage between thermodynamic state variables and the number of particles in a system [24, 47].

$$\phi = F - N\mu = -k_bTZ = -k_bT\sum_r \ln\left[1 + \exp\left(\Lambda - \frac{\varepsilon_r}{k_bT}\right)\right] \tag{9}$$

The grand partition function, Z, given in Eq. (10), can be expressed in terms of the density of states, integral expression in Eq. (10), thereby establishing a connection between thermodynamic properties and the principles of quantum statistical mechanics.

$$Z = \sum_r ln\left[1 + exp\left(\Lambda - \frac{\varepsilon_r}{k_b T}\right)\right] \approx \int_0^\infty \ln\left[1 + e^{\Lambda - \frac{\varepsilon}{k_b T}}\right] g(\varepsilon) d\varepsilon \quad (10)$$

Taking the integral in the Eq. (10), the grand partition function is obtained as follows consistent with literature [24, 47]:

$$Z = -\frac{\pi^{3/2} V}{8L_c^3} Li_{5/2}(-e^{\Lambda}) + \frac{\pi A}{4^2 L_c^2} Li_2(-e^{\Lambda}) - \frac{\sqrt{\pi} C}{2.4^2 L_c} Li_{3/2}(-e^{\Lambda}) \quad (11)$$

Therefore, the grand canonical potential assumes the following form, in agreement with the literature [24, 47]:

$$\phi = k_b T \left[\frac{\pi^{3/2} V}{8L_c^3} Li_{5/2}(-e^{\Lambda}) - \frac{\pi A}{4^2 L_c^2} Li_2(-e^{\Lambda}) + \frac{\sqrt{\pi} C}{2.4^2 L_c} Li_{3/2}(-e^{\Lambda})\right] \quad (12)$$

Eq. (12) leads us to the equation of state for Fermions [24, 47]:

$$PV = -\phi = -k_b T \left[\frac{\pi^{3/2} V}{8L_c^3} Li_{5/2}(-e^{\Lambda}) - \frac{\pi A}{4^2 L_c^2} Li_2(-e^{\Lambda}) + \frac{\sqrt{\pi} C}{2.4^2 L_c} Li_{3/2}(-e^{\Lambda})\right] \quad (13)$$

By considering L_c, Eq. (8) can be rewritten as below;

$$\tilde{n} = -Li_{3/2}(-e^{\Lambda}) \left[1 - \frac{\alpha}{\sqrt{\pi}} \frac{Li_1(-e^{\Lambda})}{Li_{3/2}(-e^{\Lambda})} + \frac{\beta}{\pi} \frac{Li_{1/2}(-e^{\Lambda})}{Li_{3/2}(-e^{\Lambda})}\right] \quad (14)$$

where, $\alpha = AL_c/2V$ and $\beta = CL_c^2/4V$, are the confinement parameters, $\tilde{n} = n_{cl}/n_q$ is the dimensionless density, $n_{cl} = N/V$ is the classical density and $n_q = 1/\lambda_{th}^3$ is the quantum density.

By rearranging Eq. (13) accordingly, the total pressure takes the following form;

$$P = -n_q k_b T Li_{5/2}(-e^{\Lambda}) \left[1 - \frac{\alpha}{\sqrt{\pi}} \frac{Li_2(-e^{\Lambda})}{Li_{5/2}(-e^{\Lambda})} + \frac{\beta}{\pi} \frac{Li_{3/2}(-e^{\Lambda})}{Li_{5/2}(-e^{\Lambda})}\right] \quad (15)$$

To understand its behavior clearly, the expression given in Eq. (15) can be made dimensionless respect to bulk (classical) degeneracy pressure of Fermi gas;

$$\frac{P}{P_{d,b}} = \tilde{P} = -\frac{5}{2\tilde{n}} \tilde{T} Li_{5/2}(-e^{\Lambda}) \left[1 - \frac{\alpha}{\sqrt{\pi}} \frac{Li_2(-e^{\Lambda})}{Li_{5/2}(-e^{\Lambda})} + \frac{\beta}{\pi} \frac{Li_{3/2}(-e^{\Lambda})}{Li_{5/2}(-e^{\Lambda})}\right] \quad (16)$$

where, $\tilde{T} = T/T_F$ is the dimensionless temperature, $T_F = \varepsilon_F/k_b$, is the Fermi (or degeneracy) temperature, $\varepsilon_F = \hbar^2(3\pi^2 n_{cl})^{2/3}/2m$ is the Fermi energy and $P_{d,b}$ is the bulk (classical) degeneracy pressure which is expressed as below [48, p.106];

$$P_{d,b} = \frac{2}{5} n_{cl} k_b T_F \quad (17)$$

Substituting Eq. (14) into Eq. (16), and using Taylor expansion while considering the smallness of the second and third terms in Eq. (14) due to α and β, the dimensionless exact total pressure expression for Fermions confined in nanoscale domains takes the form:

$$\tilde{P} = \frac{5}{2} \tilde{T} \frac{Li_{5/2}(-e^{\Lambda})}{Li_{3/2}(-e^{\Lambda})} \left[1 - \frac{\alpha^F}{\sqrt{\pi}} \sqrt{\frac{1}{\tilde{T}}} \left(\frac{Li_2(-e^{\Lambda})}{Li_{5/2}(-e^{\Lambda})} - \frac{Li_1(-e^{\Lambda})}{Li_{3/2}(-e^{\Lambda})}\right) + \frac{\beta^F}{\pi} \frac{1}{\tilde{T}} \left(\frac{Li_{3/2}(-e^{\Lambda})}{Li_{5/2}(-e^{\Lambda})} - \frac{Li_{1/2}(-e^{\Lambda})}{Li_{3/2}(-e^{\Lambda})}\right)\right] \quad (18)$$

where, $\alpha^F = \alpha/\sqrt{\Lambda_F}$, $\beta^F = \beta/\Lambda_F$, $\Lambda_F = T_F/T$ and the bulk total pressure (the pressure without QSE, $\alpha^F = \beta^F = 0$) is,

$$\tilde{P}_b = \frac{5}{2} \tilde{T} \frac{Li_{5/2}(-e^{\Lambda})}{Li_{3/2}(-e^{\Lambda})} \quad (19)$$

To obtain the thermal pressure, we need to subtract the degeneracy pressure from the total pressure. Degeneracy pressure is the pressure in the limit where the temperature approaches zero, and therefore thermal contributions disappear. Consequently, in this limit, since $\Lambda \to \infty$ or $\Lambda \gg 1$, we can use the related asymptotic behaviors of the Polylogarithmic functions. To understand the behavior of Fermi gas at low temperature regime (degenerate conditions) where $T \ll T_F$ or $\Lambda \gg 1$, all expressions including Polylogs can be re-expressed by using the

asymptotics of the Polylogs for $\Lambda \gg 1$ given in Appendix-A.

For $\Lambda \gg 1$, Eq. (14) simplifies to Eq. (20),

$$\tilde{n} = \frac{4\Lambda^{3/2}}{3\sqrt{\pi}}\left\{1 + \frac{\pi^2}{8}\frac{1}{\Lambda^2} - \frac{3}{4}\frac{\alpha}{\Lambda^{1/2}} + \frac{3}{2\pi}\frac{\beta}{\Lambda}\right\} \tag{20}$$

The dimensionless chemical potential Λ of Λ_F, in Eq. (20) is obtained inversely as below, by applying a perturbative determination method to Eq. (20) that its detail is given in the Appendix-B.

$$\begin{aligned}\Lambda &= \Lambda_F\left[1 - \frac{\pi^2}{12\Lambda_F^2} + \frac{\alpha}{2\Lambda_F^{1/2}} - \frac{\beta}{\pi\Lambda_F}\right] \\ &= \Lambda_F\left[1 - \frac{\pi^2}{12\Lambda_F^2} + \frac{\alpha^F}{2} - \frac{\beta^F}{\pi}\right]\end{aligned} \tag{21}$$

As the temperature goes to zero, $T \to 0$, then the chemical potential of a Fermi gas $\Lambda \to \Lambda_F$. Thus, to consider only the dominating terms in the asymptotical expressions of the Polylogs will be enough to reshape the total pressure to obtain the degeneracy pressure.

Under high degenerate conditions ($\Lambda \gg 1$ or $\tilde{T} \ll 1$), the total pressure given in Eq. (18) yields the asymptotical total pressure of the confined Fermi gas, $\tilde{P}_H$, as the following;

$$\begin{aligned}\tilde{P}_H = 1 &+ \frac{5\pi^2}{12}(\tilde{T})^2 - \frac{5\pi^2\alpha^F}{32}(\tilde{T})^2 \\ &+ \frac{\pi\beta^F}{2}(\tilde{T})^2 + \frac{5\alpha^F}{16}\end{aligned} \tag{22}$$

Thus, the dimensionless degeneracy pressure is obtained from Eq. (22) for $\tilde{T} \to 0$ as below;

$$\frac{P_d}{P_{d,b}} = \tilde{P}_d = 1 + \frac{5\alpha^F}{16} \tag{23}$$

Notably, the contribution from the edge correction parameter β^F vanishes in the degeneracy pressure (Eq. 23), while the surface correction α^F remains and enhances the pressure. This differential behavior has a clear physical origin: at zero temperature ($T \to 0$), only quantum states at the Fermi surface contribute to the pressure. The edge effects, which are proportional to the perimeter and scale as CL_c^2, diminish more rapidly than surface effects (proportional to AL_c) as the thermal de Broglie wavelength contracts in the low-temperature limit. Mathematically, this is evident from the polylogarithmic asymptotic expansions in Appendix A, where the L_c^2 dependence of β^F leads to higher-order corrections that vanish at $T \to 0$. In contrast, the surface term α^F directly modifies the boundary conditions at the Fermi surface, causing a persistent enhancement of degeneracy pressure by the factor $1+5\alpha^F/16$. This demonstrates that thermal and degeneracy pressures respond differently to geometric confinement, with edge effects being exclusively thermal in nature while surface effects contribute to both components.

Consequently, the exact thermal pressure for Fermions confined in nanoscale domains is obtained by subtracting the degeneracy pressure (Eq. 23) from the total pressure (Eq. 18), as shown below:

$$\begin{aligned}\frac{P_{th}}{P_{d,b}} &= \tilde{P}_{th} = \\ &\frac{5}{2}\tilde{T}\frac{Li_{5/2}}{Li_{3/2}}\left[1 - \frac{\alpha^F}{\sqrt{\pi}}\sqrt{\frac{1}{\tilde{T}}}\left(\frac{Li_2}{Li_{5/2}} - \frac{Li_1}{Li_{3/2}}\right)\right. \\ &\left. + \frac{\beta^F}{\pi}\frac{1}{\tilde{T}}\left(\frac{Li_{3/2}}{Li_{5/2}} - \frac{Li_{1/2}}{Li_{3/2}}\right)\right] - \left[1 + \frac{5\alpha^F}{16}\right]\end{aligned} \tag{24}$$

The bulk thermal pressure ($\tilde{P}_{th,b}$), defined for $\alpha^F = \beta^F = 0$, is the difference between the bulk total pressure (Eq. 19) and the bulk degeneracy pressure (Eq. 17).

$$\tilde{P}_{th,b} = \frac{5}{2}\tilde{T}\frac{Li_{5/2}}{Li_{3/2}} - 1 \tag{25}$$

where the second term represents a contribution related to the bulk degeneracy pressure ($\tilde{P}_{d,b} = 1$), which diminishes under bulk conditions ($T \gg T_F$).

The dimensionless chemical potential, Λ, used in Eq. (18), (19), (24) and (25) is obtained by numerically inverting Eq. (14). By considering the asymptotic expressions of Polylogs, asymptotical thermal pressure of the confined high degenerate Fermi gas ($\Lambda \gg 1$ or $T \ll T_F$), is obtained as below;

$$\begin{aligned}\tilde{P}_{H,th} &= \tilde{P}_H - \tilde{P}_d = \\ &\frac{5\pi^2}{12}(\tilde{T})^2 - \frac{5\pi^2\alpha^F}{32}(\tilde{T})^2 + \frac{\pi\beta^F}{2}(\tilde{T})^2\end{aligned} \tag{26}$$

Eqs. (22) and (26) are derived using the chemical potential expression given in Eq. (21).

The suppression of thermal pressure by quantum confinement revealed in Eq. (26) can be understood through the modification of the density of thermally accessible states.

In bulk systems, thermal excitations can access a continuum of states above the Fermi level. However, spatial confinement imposes boundary conditions that discretize the energy spectrum and reduce the density of states available for thermal excitation.

The confinement parameters α^F and β^F quantify this reduction: larger values correspond to stronger

confinement (smaller system dimensions relative to the thermal de Broglie wavelength), which increases the spacing between energy levels. This effectively "starves" thermal excitations of available states, suppressing the thermal contribution to pressure by terms proportional to $\alpha^F(\tilde{T})^2$ and $\beta^F(\tilde{T})^2$. Conversely, degeneracy pressure (Eq. 23) is enhanced by confinement because the Pauli exclusion principle forces fermions into higher momentum states when confined to smaller volumes. The boundary conditions effectively compress the Fermi sea into a reduced phase space, raising the Fermi energy and thus the zero-point pressure. This fundamental asymmetry, confinement suppresses thermal fluctuations while enhancing quantum statistical effects, is the central physical insight of this work and explains why total pressure measurements in confined systems cannot be interpreted without separating these contributions. By considering the asymptotical expression of Polylogs for $\Lambda \ll 1$ or $T \gg T_F$ given in Appendix-A, the total, $\tilde{P}_L$, and thermal, $\tilde{P}_{L,th}$, pressures for low degenerate Fermi gas are obtained as the following respectively;

$$\tilde{P}_L = \frac{5}{2}\tilde{T}\left[1 - \frac{\alpha^F}{\sqrt{\pi}}\sqrt{\frac{1}{\tilde{T}}}\left(\frac{-1+\sqrt{2}}{2^{5/2}}\right)exp(\Lambda) + \frac{\beta^F}{\pi}\frac{1}{\tilde{T}}\left(\frac{1}{2^{5/2}}\right)exp(\Lambda) + \left(\frac{1}{2^{5/2}}\right)exp(\Lambda)\right] \quad (27)$$

$$\tilde{P}_{L,th} = \frac{5}{2}\tilde{T}\left[1 - \frac{\alpha^F}{\sqrt{\pi}}\sqrt{\frac{1}{\tilde{T}}}\left(\frac{-1+\sqrt{2}}{2^{5/2}}\right)exp(\Lambda) + \frac{\beta^F}{\pi}\frac{1}{\tilde{T}}\left(\frac{1}{2^{5/2}}\right)exp(\Lambda) + \left(\frac{1}{2^{5/2}}\right)exp(\Lambda)\right] - \left(1 + \frac{5\alpha^F}{16}\right) \quad (28)$$

The dimensionless chemical potential used in Eqs.(27) and (28) is obtained from Eq. (14) using the asymptotic value of polylogharitms for $\Lambda \ll 1$ given in Appendix-A.

The behavior of the $\tilde{P}$ and $\tilde{P}_{th}$ (exact pressures) and the $\tilde{P}_H$, $\tilde{P}_{H,th}$, $\tilde{P}_L$ and $\tilde{P}_{L,th}$ (asymptotical pressures for high and low degeneracy regimes) are shown in Figure (1). Solid lines represent exact pressures: blue ($\tilde{P}$, total) and red ($\tilde{P}_{\text{th}}$, thermal), computed from Eqs. (18) and (24) using numerical inversion of Eq. (14) for the chemical potential. Dashed lines show asymptotic approximations for high-degeneracy regime, ($\tilde{T} < \tilde{T}^*$, Eqs. 22 and 26) and low-degeneracy regime, ($\tilde{T} > \tilde{T}^*$, Eqs. 27 and 28).

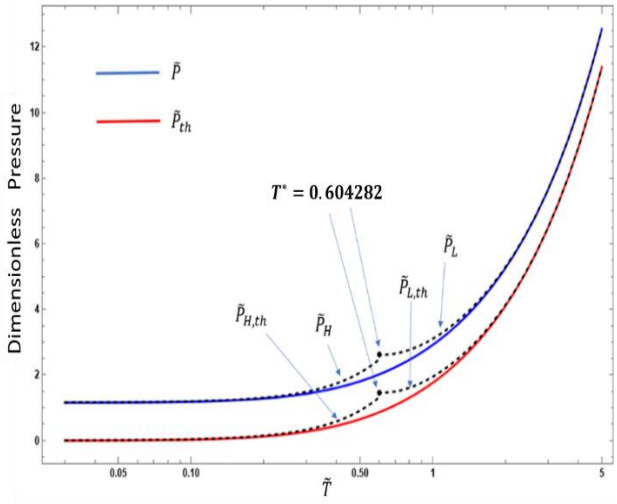

Figure 1. Comparison of exact and asymptotic expressions for total and thermal pressure of a confined Fermi gas as functions of dimensionless temperature $\tilde{T} = T/T_F$ for confinement parameters $\alpha^F = 0.2$ and $\beta^F = 0.01$

In Figure (1), it can clearly be seen that the analytical (asymptotical) total and thermal pressures for low temperatures ($\tilde{P}_H$ and $\tilde{P}_{H,th}$) represents the exact pressures for values $\tilde{T} < T^* = 0.604282$ and the analytical (asymptotical) total and thermal pressures for high temperatures ($\tilde{P}_L$ and $\tilde{P}_{L,th}$) represents the exact pressures for the values $\tilde{T} \geq T^*$, well enough. Maximum relative error for $\tilde{P}_H$ and $\tilde{P}_L$ occurs at dimensionless transition temperature, $\tilde{T} = T^*$, as 22%, while it is 52% for $\tilde{P}_{H,th}$ and $\tilde{P}_{L,th}$. Therefore, to represent $\tilde{P}$ and $\tilde{P}_{th}$ till T^*, the asymptotical expressions $\tilde{P}_H$ and $\tilde{P}_{H,th}$, and after T^*, the asymptotical expressions $\tilde{P}_L$ and $\tilde{P}_{L,th}$ can be used safely. Note that thermal pressure vanishes as $\tilde{T} \to 0$, while total pressure approaches the degeneracy pressure, confirming that $\tilde{P} = \tilde{P}_{\text{d}} + \tilde{P}_{\text{th}}$. The asymptotic forms provide accurate approximations in their respective regimes, validating the analytical expressions for practical use in confined quantum gas analysis. Figure 2 illustrates how bulk pressures ($\tilde{P}_b$ and $\tilde{P}_{th,b}$) deviate from the dimensionless exact total ($\tilde{P}$) and thermal ($\tilde{P}_{th}$) pressures of a Fermi gas under various confinement parameters (α^F and β^F).

The exact thermal pressure (red line) approaches the exact total pressure (blue line) when $\tilde{T} \gg 1$. However, they start diverging as the gas gets strongly degenerated, $\tilde{T} \ll 1$. Also, as $\tilde{T} \to 0$, thermal pressure vanishes while the total pressure approaches the degeneracy pressure as expected. Having analyzed how dimensionless pressures vary with respect to $\tilde{T}$, we can also study how these pressures change with (dimensionless) density, $\tilde{n}$.

$$\tilde{T} = \left(\frac{3\sqrt{\pi}}{4}\right)^{-2/3}\tilde{n}^{-2/3} \quad (29)$$

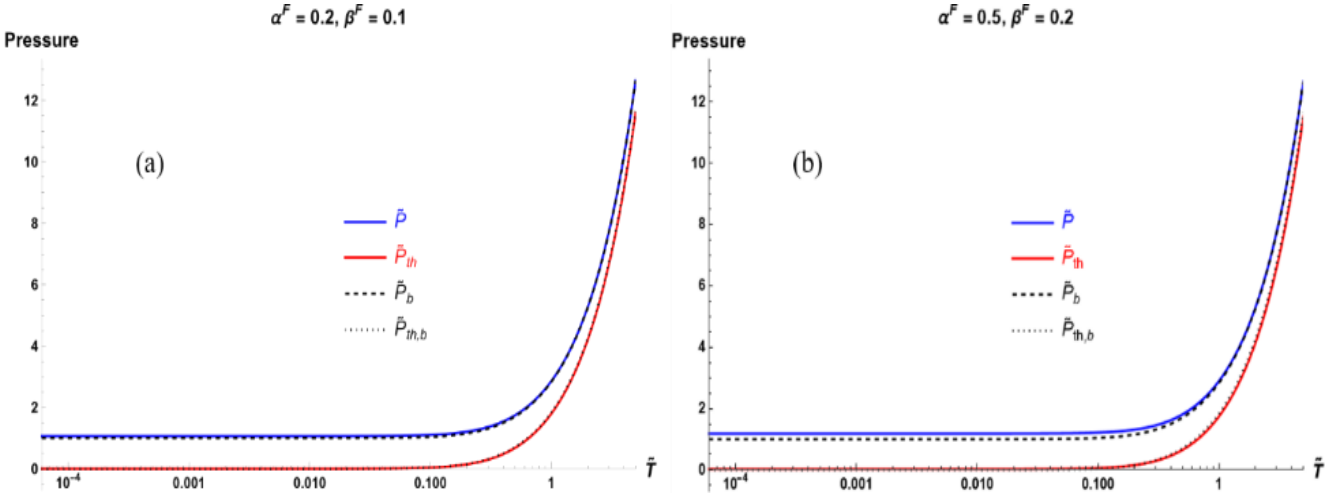

Figure 2. Deviation of bulk pressure expressions ($\tilde{P}_b, \tilde{P}_{th,b}$) from exact confined pressure expressions ($\tilde{P}$, $\tilde{P}_{th}$) versus dimensionless temperature $\tilde{T}$ for two confinement parameter sets: (a) $\alpha^F = 0.2$, $\beta^F = 0.01$ (moderate confinement) and (b) $\alpha^F = 0.5$, $\beta^F = 0.2$ (strong confinement). Blue solid line: exact total pressure (Eq. 18); blue dashed line: bulk total pressure (Eq. 19, no quantum size effects). Red solid line: exact thermal pressure (Eq. 24); red dashed line: bulk thermal pressure (Eq. 25, $\alpha^F = \beta^F = 0$)

The relationship in Eq. (29) provides another way to understand the degeneracy behavior of a Fermi gas, as illustrated in Figure 3. From the definition of Fermi energy, ε_F, the relationship between the dimensionless temperature, $\tilde{T}$ and the dimensionless density, $\tilde{n}$, is obtained as the following; Solid lines represent exact expressions from Eqs. (18), (24), and (23). Dashed lines show asymptotic approximations for high degeneracy ($\tilde{n} > \tilde{n}^*$, Eqs. 22, 26) and low degeneracy ($\tilde{n} < \tilde{n}^*$, Eqs. 27, 28). Blue curves refers total pressure $\tilde{P}$ and red curves, thermal pressure $\tilde{P}_{\text{th}}$. The double-logarithmic representation emphasizes the divergence between exact and bulk expressions at low densities (high $\tilde{T}$, classical limit) and reveals the power-law behavior $\tilde{P}_{\text{th}} \propto \tilde{n}^{(2/3)}$ in the degenerate regime. The transition density $\tilde{n}^*$ corresponds to $\tilde{T}^* \approx 0.604282$ via Eq. (28).

At high densities ($\tilde{n} \gg 1$), the Fermi gas becomes strongly degenerate: thermal pressure vanishes ($\tilde{P}_{\text{th}} \to 0$), and total pressure approaches degeneracy pressure ($\tilde{P} \to \tilde{P}_{\text{d}}$). At low densities ($\tilde{n} \ll 1$), thermal pressure dominates, and both $\tilde{P}$ and $\tilde{P}_{\text{th}}$ approach the classical limit (Eqs. 31, 32).

This representation complements Figure 2 by showing how pressure scales with density, a key parameter in experimental systems where particle number and volume are controlled independently.

For classical gases ($\Lambda \to -\infty$), since;

$$Li_m(-e^{\Lambda}) \to -e^{\Lambda} \tag{30}$$

Then, the total and thermal bulk pressures for classical gases is obtained from Eq.(19) and Eq. (25) as below respectively;

$$\tilde{P}_{b,cl} = \frac{5}{2}\tilde{T} \to P_{b,cl} = \frac{5}{2}\frac{T}{T_F}P_{d,b} = n_{cl}k_bT \tag{31}$$

$$\tilde{P}_{th,b,cl} = \frac{5}{2}\tilde{T} - 1 = \tilde{T}\left(\frac{5}{2} - \frac{1}{\tilde{T}}\right) \xrightarrow{\tilde{T}\to\infty} P_{th,b,cl} = \frac{5}{2}\frac{T}{T_F}P_{d,b} = n_{cl}k_bT \tag{32}$$

3. Discussion: scope, limitations, and extensions

While this study provides a comprehensive theoretical framework for separating thermal and degeneracy pressure in confined Fermi gases, several assumptions and limitations should be noted, along with directions for future work.

3.1. Ideal Gas Approximation and Interaction Effects

The present analysis assumes non-interacting fermions obeying ideal Fermi-Dirac statistics. In real systems, interactions, such as Coulomb repulsion in electron gases or contact interactions in ultracold atoms, can modify both thermal and degeneracy contributions. For weakly interacting systems, mean-field theories (e.g., Hartree-Fock) could extend our framework by renormalizing the effective Fermi energy and introducing interaction-dependent corrections to the pressure.

In strongly correlated regimes, more sophisticated approaches like dynamical mean-field theory or quantum Monte Carlo simulations would be required. However, our ideal gas results provide a necessary baseline for interpreting interaction effects: deviations from Eqs. (18), (23) and (24) in experimental measurements can diagnose the strength and nature of interactions in confined geometries.

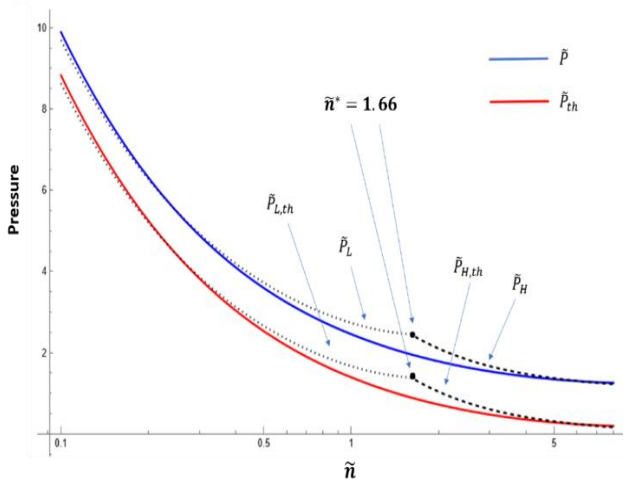

Figure 3. Pressure components versus dimensionless particle density $\tilde{n} = n_{cl}/n_q$ for a confined Fermi gas with $\alpha^F = 0.2$ and $\beta^F = 0.01$

3.2. Dimensional Generalization: 2D and 1D Systems

This work focuses on three-dimensional confinement, but many experimental platforms, such as graphene (2D), quantum wires (1D), and quantum dots (0D), operate in reduced dimensionalities.

The Weyl-based density of states (Eq. 5) generalizes straightforwardly to 2D and 1D by retaining only the relevant geometric terms in Eq. (3). For example, in 2D, only area (A) and perimeter (C) terms survive, simplifying the confinement parameter structure. Preliminary analysis suggests that the thermal-degeneracy separation remains conceptually intact, but the enhancement factors and asymptotic forms differ quantitatively. A systematic study of dimensional crossover effects is planned for future work, particularly for quasi-2D systems where one dimension is tightly confined while others remain extended.

3.3. Validity of Weyl's Conjecture for Irregular Boundaries

Weyl's asymptotic eigenvalue formula (Eq. 3) assumes smooth, piecewise-differentiable boundaries. For domains with fractal or highly irregular boundaries, higher-order corrections beyond surface and edge terms may be necessary [31, 37].

In such cases, the confinement parameters α and β become geometry-dependent in non-trivial ways, potentially introducing additional length scales.

However, for most experimentally relevant nanostructures, rectangular quantum wells, cylindrical nanowires, spherical quantum dots, the smooth boundary approximation is excellent. Extensions to rough boundaries could incorporate disorder-averaged density of states, relevant for realistic material interfaces.

3.4. Experimental Accessibility and Measurement Strategies

A central motivation for this work is that experiments typically measure only total pressure (or related quantities like compressibility, chemical potential, or equation of state parameters).

Our decomposition into thermal and degeneracy components is not directly observable but enables interpretation of measurements as follows:

1. Temperature-Dependent Measurements: By varying T at fixed particle number N and measuring $P(T)$, one can fit Eq. (18) to extract α^F and β^F. The low-temperature limit yields P_d (Eq. 23).
2. Ultracold Atomic Gases: In optical lattices or harmonic traps, the effective confinement parameters can be tuned by adjusting laser intensities.

Our predictions could be tested by measuring the density profile via absorption imaging and extracting pressure through the local density approximation [7].

3. Nanoelectronic Devices: In 2D electron gases (e.g., GaAs/AlGaAs heterostructures) or quantum dots, capacitance spectroscopy probes the density of states, from which pressure can be inferred thermodynamically [55]. Comparison with our Eqs. (22)-(24) could validate QSE predictions.

3.5. Comparison to Bose Gases

While this study focuses on fermions, a parallel analysis for confined Bose gases would reveal complementary physics.

In Bose-Einstein condensates, degeneracy pressure can become negative (attractive effective pressure due to ground state macroscopic occupation), contrasting sharply with the repulsive fermionic degeneracy pressure. The thermal component in bosonic systems would similarly be suppressed by confinement, but the interplay with condensate depletion introduces additional complexity [1, 6]. A comparative study of fermionic vs. bosonic confined gases is a natural extension.

3.6. Higher-Order Corrections and Convergence

Our asymptotic expansions retain terms up to $O(A^{-2})$ for high degeneracy (Appendix A, Eq. A.3) and leading exponential terms for low degeneracy (Eq. A.1). The error analysis (Figure 1) shows that these truncations yield <22% error at the transition point only for total pressure. For higher-precision applications, next-order terms (e.g., $O(A^{-4})$ corrections in the Sommerfeld expansion [53]) could be included, though at the cost of analytical complexity.

Convergence of the polylogarithmic series has been rigorously established [50], ensuring our expressions are asymptotically exact in their respective limits.

3.7. Future Directions

Key extensions include: (1) incorporating weak interactions via perturbation theory or mean-field approaches; (2) generalizing to 2D/1D and studying dimensional crossover; (3) comparing predictions to high-precision experiments in ultracold atoms and quantum dots; (4) exploring time-dependent thermodynamics (e.g., pressure relaxation after quenches in trap geometry); and (5) analyzing bosonic analogs to establish universal principles of confinement-induced pressure modification across quantum statistics.

4. Conclusion

This study establishes a refined thermodynamic framework for Fermi gases confined to nanoscale domains by explicitly disentangling total pressure into thermal and degeneracy components. While total pressure is the experimentally accessible quantity, our decomposition, achieved by subtracting the zero-temperature limit from polylogarithmic expressions derived via Weyl's density of states, reveals that spatial confinement impacts these components in fundamentally different ways.

The central result is that quantum size effects, parameterized by α^F (surface-to-volume) and β^F (edge-to-volume) ratios, enhance degeneracy pressure by $(1 + 5\alpha^F/16)$ while suppressing thermal pressure through terms proportional to $(\alpha^F.\tilde{T}^2)$ and $(\beta^F.\tilde{T}^2)$. This differential response arises because confinement restricts thermally accessible states while simultaneously compressing the Fermi sea, raising zero-point pressure. Notably, edge effects (β^F) contribute only to thermal pressure and vanish at $T \to 0$, whereas surface effects (α^F) modify both components but dominate the degeneracy pressure.

We have derived exact expressions (Eqs. 18, 24) valid across all degeneracy regimes and asymptotic forms for high (strong) ($T \ll T_F$, Eqs. 22, 26) and low (weak) ($T \gg T_F$, Eqs. 27, 28) degeneracy, with validated relative errors below 22% for total pressure and 52% for thermal pressure at the transition temperature $\tilde{T}^* \approx 0.604282$. These analytical expressions enable rapid evaluation without numerical integration of polylogarithms, facilitating application to experimental data analysis. The framework clarifies how to interpret thermodynamic measurements in confined systems where only total pressure is observable. By fitting temperature-dependent pressure data to our expressions, one can extract confinement parameters and separately quantify thermal versus quantum statistical contributions. This has direct implications for: (1) ultracold atomic gases in optical lattices, where trap geometry can be tuned to test QSE predictions; (2) nanoelectronic devices, where understanding pressure contributions aids in thermal management and device design; and (3) quantum dots and nanowires, where thermodynamic properties govern charge and heat transport. Future extensions should address interaction effects beyond the ideal gas approximation, generalize to lower-dimensional systems (2D/1D), and compare predictions to high-precision experiments. The differential impact of confinement on thermal versus degeneracy pressure established here provides a foundation for understanding how boundaries modify thermodynamics in the growing landscape of quantum-confined technologies.

Funding Declaration

The author(s) received no financial support for the research

Authors Contribution
As the sole author, I have participated sufficiently in the intellectual content, conception, and design of this work, as well as the analysis and interpretation of the data and the writing of the manuscript.

Availability of data and materials
No Data associated in the manuscript

Conflict of interests
Author declares that no conflicts of interest.

References

[1] Andreev P. A., Mosaki I. N., Trukhanova M. Iv. (2021). Quantum hydrodynamics of the spinor Bose–Einstein condensate at non-zero temperatures. *Physics of Fluids* 33:6, 067108, doi: https://doi.org/10.1063/5.0053035

[2] Fischer H., Käding C., Pitschmann M. (2025). Quantum and thermal pressures from light scalar fields, *Physics of the Dark Universe*, 47, 101756, doi: https://doi.org/10.1016/j.dark.2024.101756 https://doi.org/10.1007/s10649-011-9307-4

[3] Angel, R. J., Miozzi, F., & Alvaro, M. (2019). Limits to the Validity of Thermal-Pressure Equations of State. *Minerals*, 9:9, 562. doi: https://doi.org/10.3390/min9090562

[4] Ahmed Mohamed, E., Ali Ahmed, N., Babiker Hussein, M., Mohammad Taha, R., Ahmed, M. and Abd-Alla, M. (2020). Explanation of Pressure Effect for High Temperature Superconductors Using Pressure Dependent Schrodinger Equation and String Theory. *Natural Science*, 12, 28-34. doi: https://doi.org/10.4236/ns.2020.121004

[5] Yan, J., Yang, S., (2022). Thermal Pressure in the Thermal Equation of State for Solid and a Proposed Substitute. *Int J Thermophys* 43, 169, doi: https://doi.org/10.1007/s10765-022-03089-8

[6] Kuznietsov V. A., Savchuk O., Stashko O. S., Gorenstein M. I. (2022). Critical point influenced by Bose-Einstein condensation, *Phys. Rev. C*, 106, 034319, doi: https://doi.org/10.1103/PhysRevC.106.034319

[7] Fenech, K., Dyke, P., Peppler, T., Lingham, M., Hoinka, S., Hu, H., & Vale, C.J. (2015). Thermodynamics of an Attractive 2D Fermi Gas. *Phys. Rev. Lett*., 116 4, 045302. doi: https://doi.org/10.1103/PhysRevLett.116.045302

[8] Dai, W.S., and Xie, M. (2004). Geometry effects in confined space, *Phys. Rev. E*. 70, 016103. doi: https://doi.org/10.1103/PhysRevE.70.016103

[9] Sisman, A., Muller, I. (2004). The Casimir-like size effects in ideal gases, *Phys. Lett. A*, 320:5–6, 360-366, doi: https://doi.org/10.1016/j.physleta.2003.11.054

[10] Sisman, A. (2004). Surface dependency in thermodynamics of ideal gases, *J. Phys. A: Math. Gen*., 37, 11353, doi: https://doi.org/10.1088/0305-4470/37/47/004

[11] Sisman, A., Ozturk, Z.F., Firat, C. (2007). Quantum boundary layer: a non-uniform density distribution of an ideal gas in thermodynamic equilibrium, *Phys. Lett. A*, 362:1, 16-20, doi: https://doi.org/10.1016/j.physleta.2006.09.083

[12] Firat, C., and Sisman, A. (2009). Universality of the quantum boundary layer for a Maxwellian gas, *Phys. Scr.*, 79, 2009) 065002, doi: https://doi.org/10.1088/0031-8949/79/06/065002

[13] Ozturk, Z.F. and Sisman, A. (2009). Quantum size effects on the thermal and potential conductivities of ideal gases, *Phys. Scr*., 80, 06540, doi: https://doi.org/10.1088/0031-8949/80/06/065402

[14] Firat, C. Sisman, A., Ozturk, Z.F. (2010). Thermodynamics of gases in nano cavities, *Energy*, 35:2, 814-819, doi: https://doi.org/10.1016/j.energy.2009.08.020

[15] Firat, C., Sisman, A., and Ozturk, F. (2011). Effects of Particle-Wall Interactions on the Thermodynamic Behavior of Gases at the Nano Scale, Int. J. of Thermodynamics, 14:4, 155–161, doi: https://doi.org/10.5541/ijot.317

[16] Ozturk, Z. Sisman, A. and Firat, C. (2011). Gas Diffusion at the Nano Scale, *Int. J. of Thermodynamics*, 14:4, 163–166. doi: https://doi.org/10.5541/ijot.316

[17] Sisman, A., Babac, G. (2012). Quantum size effects on classical thermosize effects, *Continuum Mech. Thermodyn.*, 24, 339–346, doi: https://doi.org/10.1007/s00161-011-0214-9

[18] Firat, C. and Sisman, A. (2013). Quantum forces of a gas confined in nano structures, *Phys. Scr*., 87, 045008, doi: https://doi.org/10.1088/0031-8949/87/04/045008

[19] Aydin, A. and Sisman, A. (2014). Discrete nature of thermodynamics in confined ideal Fermi gases, *Phys. Lett. A*, 378: 30-31, doi: https://doi.org/10.1016/j.physleta.2014.05.044

[20] Aydin, A. and Sisman, A. (2015). Dimensional transitions in thermodynamic properties of ideal MB gases, *Phys. Scr*., 90:4, 045208, doi: https://doi.org/10.1088/0031-8949/90/4/045208

[21] Dai, W.S., Xie, M. (2003). Quantum statistics of ideal gases in confined space, *Phys. Lett. A*, 311:4–5, 340-346. doi: https://doi.org/10.1016/S0375-9601(03)00510-3

[22] Firat, C., Sisman, A. and Aydin, A. (2018). Characterization of density oscillations in confined and degenerate Fermi gases, *Modern Phys. Lett. B*, 32:32, 1850393, doi: https://doi.org/10.1142/S0217984918503931

[23] Aydin, A., and Sisman, A. (2019). Quantum shape effects and novel thermodynamic behaviors at nanoscale, *Phys. Lett. A*, 383:7, 655-665, doi: https://doi.org/10.1016/j.physleta.2019.01.009

[24] Pang, H. Dai, W.-S., and Xie, M. (2011). The pressure exerted by a confined ideal gas, *J. Phys. A: Math. Theor*. 44, 365001, doi: https://doi.org/10.1088/1751-8113/44/36/365001

[25] Pathria R.K. and Beale P.D. (2011). *Statistical Mechanics*, 3rd ed. Pergamon Press

[26] Weyl, H. (1911). *Ueber die asymptotische Verteilung der Eigenwerte*, Nachrichten von der Gesellschaft der Wissenschaften zu Göttingen, Mathematisch-Physikalische Klasse, 110-117.

[27] Kac, M. (1966). Can one hear the shape of a drum? The *Am. Math. Monthly*, 73, 1-23. doi: https://doi.org/10.1080/00029890.1966.11970915

[28] Zayed, E.M.E. (2000). Inverse problem for a bounded domain in R3 with piecewise smooth mixed boundary conditions, *Int. J. Theor. Phys*., 39, 189-205. doi: https://doi.org/10.1023/A:1003663621045

[29] Zayed, E.M.E. (1994). On hearing the shape of rectilinear regions, *J. Math. Phys*., 35, 3490-3496. doi: https://doi.org/10.1063/1.530480

[30] Lapidus, M.L. (1991). Fractal drum, Inverse spectral problems for elliptic operators and a partial resolution of the Weyl-Berry conjecture, *Trans. of the Am. Math. Soc*., 325, 465-529. doi: https://doi.org/10.1090/S0002-9947-1991-0994168-5

[31] Vassiliev, D. and Safarov, Y. (1996*). The asymptotic distribution of eigenvalues of partial differential operators*, Providence R.I., American Mathematical Society. Softcover ISBN: 978-0-8218-0921-1.

[32] Clark, C. (1967). The asymptotic distribution of eigenvalues and eigenfunctions for elliptic boundary problems, *SIAM Rev*., 9, 627-646. doi: https://doi.org/10.1137/1009105

[33] Baltes, H. P. (1972). Asymptotic eigenvalue distribution for the wave equation in a cylinder of arbitrary cross section, *Phys. Rev. A*, 6, 2252-2257. doi: https://doi.org/10.1103 /PhysRevA.6.2252

[34] Chaba, A.N. and Pathria, R.K. (1973). Edge and curvature effects in Weyl's problem, *Phys. Rev. A*. 8, 3264-3265. doi: https://doi.org/10.1103/PhysRevA.8.3264

[35] Ivrii, V.Ya. (1980). On the second term of the spectral asymptotics for the Laplace-Beltrami operator on manifolds with boundary, *English transl. in Functional Anal. Appl.*, 14, 98–106.

[36] Netrusov, Yu, and Safarov, Yu. (2003). Weyl asymptotic formula for the Laplacian on domains with rough boundaries, *Commun. Math. Phys*. 253, 481-509. doi: https://doi.org/10.1007/s00220-004-1158-8.

[37] Potempa, H. and Schweitzer, L. (1998). Dependence of critical level statistics on the sample shape, *J. Phys.: Condens. Matter* 10 L431. doi: https://doi.org/10.1088/0953-8984/10/25/003

[38] Braun, D., Montambaux, G., and Pascaud, M. (1998). Boundary Conditions at the Mobility Edge, *Phys. Rev. Lett*. 81, 1062. doi.org/10.1103/PhysRevLett.81.1062

[39] Kravtsov, V.E. and Yudson, V.I. (1999). Topological Spectral Correlations in 2D Disordered Systems, *Phys. Rev. Lett.* 82, 157. doi: https://doi.org/10.1103/PhysRevLett.82.157

[40] Aydin, A., Sisman, A., (2016). Discrete density of states, *Phys. Lett. A*, 380, 1236–1240. doi: https://doi.org/10.1016/j.physleta.2016.01.034

[41] Dai, W.-S., and Xie, M. (2009). The number of eigenstates: counting function and heat kernel, *J. of High Energy Phys*., 2009, doi: https://doi.org/10.1088/1126-6708/2009/02/033

[42] Aydin, A., Oikonomou, T., Bagci, G.B., and Sisman, A. (2019). Discrete and Weyl density of states for photonic dispersion relation, *Phys. Scr*., 94, 105001, doi: https://doi.org/10.1088/1402-4896/ab0bc5

[43] Aydin, A., Sisman, A. (2023). Origin of the quantum shape effect, *Phys. Rev. E*, 108, 024105, doi: https://doi.org/10.1103/PhysRevE.108.024105

[44] Abramowitz M. and Stegun, C.A. (1972). *Handbook of Mathematical Functions with Formulas, Graphs, and Mathematical Tables*, Dover Publications, New York. ISBN-10: 0486612724.

[45] Prudnikov, A.P. (1980). *Integrals and Series*, Vol.3, Gordon and Breach, NY, USA. eBook ISBN9780203750643.

[46] Dai, W.-S., and Xie, M. (2007). Interacting quantum gases in confined space: Two- and three-dimensional equations of state, *J. of Math. Phys*., 48, 123302, doi: https://doi.org/10.1063/1.2821248

[47] Fitzpatrick, R., (2024). Introductory Quantum Mechanics, LibreTexts, TX, USA.

[48] Huang, K. (1991). *Statistical Mechanics*, 2nd Ed., John Wiley and Sons, NY, USA. ISBN-10:0471815187.

[49] D. Wood, 1992. *The computation of polylogarithms, Technical Report* 15-92*, University of Kent, Computing Laboratory, Canterbury, UK

[50] PolyLog, 2025. /PolyLog.pdf, Accessed on 17.04.2025 doi: https://functions.wolfram.com/PDF

[51] Fukushima, T. (2014). Computation of a general integral of Fermi–Dirac distribution by McDougall–Stoner method, *Applied Mathematics and Computation* 238, 485–510, doi: https://doi.org/10.1016/j.amc.2014.04.028

[52] Selmke, M. (2007). *The Sommerfeld Expansion*, Universität Leipzig, Department of Physics, https://s5512bfc73818070c.jimcontent.com/download/version/1418743530/module/5512592980/name/SommerfeldExpansion.pdf, Accessed on 18.04.2025.

[53] Ashcroft, N.W., and Mermin, N.D. (2011). *Solid State Physics*, Cengage Learning, ISBN 813150052.

[54] Kariminezhad, F., Rajaei, E., Fali, A., & Mirzaei, R. (2016). Impact of gain compression factor on

modulation characteristics of InGaAs/GaAs self-assembled quantum dot lasers. *J Theor Appl Phys* 10, 281–287.
doi: https://doi.org/10.1007/s40094-016-0227-7

[55] Tshipa, M. (2017). Electron states in a sinusoidally deformed cylindrical quantum wire. *J Theor Appl Phys* 11, 151–155.
doi: https://doi.org/10.1007/s40094-017-0245-0

Appendix-A: Series expansions of Polylogarithm functions

The asymptotics of Polylogs for $\Lambda \ll 1$ or $T \gg T_F$ or $(\Lambda \to -\infty)$:

$$Li_m(-e^{\Lambda}) \approx -e^{\Lambda} + \frac{e^{2\Lambda}}{2^m} - \frac{e^{3\Lambda}}{3^m} + \cdots \tag{A.1}$$

The asymptotes of polylogarithm functions for $\Lambda \gg 1$ or $T \ll T_F$

$$Li_{m+1}[-exp(\Lambda)] \cong -\frac{1}{m\Gamma(m)}\left[\frac{\Lambda^{m+1}}{m+1} + \frac{\pi^2}{6}m\Lambda^{m-1} + O(4)\right] \tag{A.2}$$

These expansions are derived via the Sommerfeld expansion method, detailed in [53, 54], which systematically expands Fermi-Dirac integrals in powers of $(k_bT/\varepsilon_F)^2$ for degenerate systems.

$$Li_{m+1}[-exp(\Lambda)] \cong -\frac{\Lambda^{m+1}}{\Gamma(m+2)}\left[1 + \frac{\pi^2}{6}\frac{1}{\Lambda^2}(m+1)m + \frac{7\pi^4}{360}\frac{1}{\Lambda^4}(m+1)m(m-1)(m-2) + O(6)\right] \tag{A.3}$$

The general formula in Eq. (A.3), retaining higher-order terms, follows from contour integration techniques for polylogarithms documented in [50] and thermal physics references [25, 49, 51]. For computational implementations, see [52] for robust numerical evaluation algorithms.

If we consider only the first two terms, then the asymptotes of some of the polylogarithm functions are;

$$Li_{5/2}[-exp(\Lambda)] \cong -\frac{8\Lambda^{\frac{5}{2}}}{15\sqrt{\pi}}\left[1 + \frac{5\pi^2}{8}\frac{1}{\Lambda^2}\right] \tag{A.4}$$

$$Li_2[-exp(\Lambda)] \cong -\frac{\Lambda^2}{2}\left[1 + \frac{\pi^2}{3}\frac{1}{\Lambda^2}\right] \tag{A.5}$$

$$Li_{3/2}[-exp(\Lambda)] \cong -\frac{4\Lambda^{\frac{3}{2}}}{3\sqrt{\pi}}\left[1 + \frac{\pi^2}{8}\frac{1}{\Lambda^2}\right] \tag{A.6}$$

$$Li_1[-exp(\Lambda)] \cong -\Lambda - exp(-\Lambda) \cong -\Lambda \tag{A.7}$$

$$Li_{1/2}[-exp(\Lambda)] \cong -\frac{2\Lambda^{\frac{1}{2}}}{\sqrt{\pi}}\left[1 - \frac{\pi^2}{24}\frac{1}{\Lambda^2}\right] \tag{A.8}$$

Error in these expansions is in the order of 10^{-4} even for $\Lambda = 10$.

10.57647/jtap.2026.2002.15

Appendix-B: Perturbative derivation of Λ under degenerate conditions in 3D

For Eq. (8), if we set the confinement parameters as:

$$\alpha = L_c \frac{A}{2V}, \quad \beta = L_c^2 \frac{C}{4V} \tag{B.1}$$

Then, the Eq. (8) takes the following form;

$$N = -\frac{\pi^{3/2} V}{8L_c^3} Li_{3/2}(-e^{\Lambda}) \left[1 - \frac{\alpha}{\sqrt{\pi}} \frac{Li_1(-e^{\Lambda})}{Li_{3/2}(-e^{\Lambda})} + \frac{\beta}{\pi} \frac{Li_{1/2}(-e^{\Lambda})}{Li_{3/2}(-e^{\Lambda})}\right] \tag{B.2}$$

By using the asymptotes of the Polylogs given in Appendix-A, Eq. (B.2) can be rewritten as below;

$$N = \zeta_c \frac{4\Lambda^{3/2}}{3\sqrt{\pi}} \left[1 + \frac{\pi^2}{8} \frac{1}{\Lambda^2} - \frac{3\alpha}{4\Lambda^{1/2}} + \frac{3}{2\Lambda} \frac{\beta}{\pi}\right] = \zeta_c \tilde{N} \tag{B.3}$$

where, ζ_c is the single particle partition function:

$$\zeta_c = \frac{\pi^{\frac{3}{2}} V}{8L_c^3} \tag{B.4}$$

For $\Lambda \gg 1$, by ignoring the size effects ($\alpha = 0, \beta = 0$) in the bracket, we can obtain the dimensionless chemical potential for Fermi particles, Λ_F;

$$N \approx \zeta_c \frac{4\Lambda_F^{\frac{3}{2}}}{3\sqrt{\pi}} \Rightarrow \Lambda_F = \frac{\mu_F}{k_b T} = \left(\frac{3\sqrt{\pi} N}{4\zeta_c}\right)^{\frac{2}{3}} = \left(\frac{3n_{cl}}{4g_s\pi}\right)^{\frac{2}{3}} \frac{h^2}{2mk_b T} \tag{B.5}$$

where, classical density:

$$n_{cl} = \frac{N}{V} \tag{B.6}$$

From Eq. (B.3);

$$\frac{N}{\zeta_c} = \tilde{N} = \frac{4}{3\sqrt{\pi}} \Lambda^{3/2} + \frac{\pi^{3/2}}{6\Lambda^{1/2}} - \frac{\alpha}{\sqrt{\pi}} \Lambda + \frac{2\beta}{\pi^{3/2}} \Lambda^{1/2} \tag{B.7}$$

$$\tilde{N} \approx ax^3 + bx^2 + c\,x + \frac{d}{x} \tag{B.8}$$

Here, $x = \Lambda^{1/2}$, $a = \frac{4}{3\sqrt{\pi}}$, $b = -\frac{\alpha}{\sqrt{\pi}}$, c=$\frac{2\beta}{\pi^{3/2}}$, and $d = \frac{\pi^{3/2}}{6}$.

$$\tilde{N}x \approx ax^4 + bx^3 + c\,x^2 + d \tag{B.9}$$

In Eq. (B.9), for $x \gg 1$, since;

$$ax^4 \gg bx^3, \quad ax^4 \gg c\,x^2 \text{ and } ax^4 \gg d \tag{B.10}$$

Then, Eq. (B.9) can be written approximately and the approximate solution of the equation, x', is found as;

$$\tilde{N}x' \approx ax'^4 \Rightarrow x' = \left(\frac{\tilde{N}}{a}\right)^{1/3} \tag{B.11}$$

Hence, the real solution will be found by the perturbative process as the following;

$$x = x' + \delta x \tag{B.12}$$

By inserting (B.12) into (B.9), one can obtain δx;

$$\tilde{N}.(x'+\delta x) \approx a(x'+\delta x)^4 + b(x'+\delta x)^3 + c(x'+\delta x)^2 + d \tag{B.13}$$

$$\tilde{N}x' + \tilde{N}\delta x \approx ax'^4 + 4ax'^3\delta x + bx'^3 + 3bx'^2\delta x + cx'^2 + 2cx'\delta x + d + \sigma(\delta x^2) \tag{B.14}$$

Since δx is too small, then $\sigma(\delta x^2)$ can be ignored.

$$\delta x \approx \frac{\tilde{N}x' - ax'^4 - bx'^3 - cx'^2 - d}{4ax'^3 + 3bx'^2 + 2cx' - \tilde{N}} \overset{ax'^4 \approx \tilde{N}x'}{\cong} -\frac{bx'^3 + cx'^2 + d}{4ax'^3 + 3bx'^2 + 2cx' - \tilde{N}} \tag{B.15}$$

$$\delta x \approx -x' \frac{bx'^2 + cx' + \frac{d}{x'}}{4ax'^3 + 3bx'^2 + 2cx' - \left[ax'^3 + bx'^2 + c\,x' + \frac{d}{x'}\right]} = -x' \frac{bx'^2 + cx' + \frac{d}{x'}}{3ax'^3 + 2bx'^2 + cx' - \frac{d}{x'}} \tag{B.16}$$

$$x = x' + \delta x = x'\left[1 - \frac{bx'^2 + cx' + \frac{d}{x'}}{3ax'^3 + 2bx'^2 + cx' - \frac{d}{x'}}\right] = x' \frac{\left[1 + \frac{b}{3ax'} - \frac{2d}{3ax'^4}\right]}{\left[1 + \frac{2b}{3ax'} + \frac{c}{3ax'^2} - \frac{d}{3ax'^4}\right]} \tag{B.17}$$

Thus, the solution for (B.9) is obtained as below:

$$x = x' \frac{\left[1 - \frac{\alpha}{4x'} - \frac{\pi^2}{12x'^4}\right]}{\left[1 - \frac{\alpha}{2x'} + \frac{\beta}{2\pi x'^2} - \frac{\pi^2}{24x'^4}\right]} \tag{B.18}$$

Eq. (B.18) can be rewritten by making use of Taylor expansion, $\frac{1}{1+\varepsilon} \approx 1 - \varepsilon$;

$$x = x' \frac{\left[1 - \frac{\alpha}{4x'} - \frac{\pi^2}{12x'^4}\right]}{\left[1 - \frac{\alpha}{2x'} + \frac{\beta}{2\pi x'^2} - \frac{\pi^2}{24x'^4}\right]} \approx x'\left[1 - \frac{\alpha}{4x'} - \frac{\pi^2}{12x'^4}\right]\left[1 + \frac{\alpha}{2x'} - \frac{\beta}{2\pi x'^2} + \frac{\pi^2}{24x'^4}\right] \tag{B.19}$$

By ignoring the small terms including α^2, $\alpha\beta$ and $\sigma\left(\frac{1}{x'^5}\right)$, Eq. (B.19) takes the form of;

$$x \approx x'\left[1 + \frac{\alpha}{4x'} - \frac{\beta}{2\pi x'^2} - \frac{\pi^2}{24x'^4}\right] \tag{B.20}$$

Considering (B.5) and (B.11), x' obtained as;

$$x' = \Lambda_F^{1/2} \tag{B.21}$$

Thus, the Eq. (B.20) is written as the following;

$$\Lambda^{1/2} = \Lambda_F^{1/2}\left[1 + \frac{\alpha}{4\Lambda_F^{1/2}} - \frac{\beta}{2\pi\Lambda_F} - \frac{\pi^2}{24\Lambda_F^2}\right] \tag{B.22}$$

If we set $\alpha^F = \alpha/\sqrt{\Lambda_F}$ and $\beta^F = \beta/\Lambda_F$ and make use of Taylor expansion for the square of (B.22), then the dimensionless chemical potential is obtained as below:

$$\Lambda = \Lambda_F\left[1 - \frac{\pi^2}{12\Lambda_F^2} + \frac{\alpha^F}{2} - \frac{\beta^F}{\pi}\right] \tag{B.23}$$